HHS Public Access

Author manuscript

Int J Pharm. Author manuscript; available in PMC 2022 September 25.

Published in final edited form as:

Int J Pharm. 2021 September 25; 607: 120972. doi:10.1016/j.ijpharm.2021.120972.

Near-infrared Light Triggered Activation of Pro-drug Combination Cancer Therapy and Induction of Immunogenic Cell Death

Xuejia Kang[1], **Yuxin Cai**[2], **Qi Wang**[1], **Chuanyu Wang**[2], **Wu Chen**[1], **Wen Yang**[2], **Amol Suryawanshi**[3], **Gang Zhou**[4], **Pengyu Chen**[2], **Feng Li**[1,*]

[1]Department of Drug Discovery and Development, Harrison School of Pharmacy, Auburn University, Auburn, AL, 36849 USA

[2]Materials Research and Education Center, Materials Engineering, Department of Mechanical Engineering, Auburn University, Auburn, AL, 36849 USA

[3]Department of Pathobiology, College of Veterinary Medicine, Auburn University, Auburn, AL, 36849 USA

[4]Georgia Cancer Center, Medical College of Georgia, Augusta University, Augusta, GA, 30912 USA.

Abstract

Disulfiram copper complex [$Cu(DDC)_2$] nanoparticles have been explored as promising anticancer agents but with concerns of toxic side effects. To improve tumor specificity and enhance anticancer efficacy, we developed a novel [copper sulfide nanoparticle (CuS NP) + disulfiram prodrug (DQ) micelle + near-infrared (NIR) laser] (CDL) combination therapy. DQ, a reactive oxygen species (ROS)-responsive prodrug, can be selectively activated at the tumor site with elevated ROS to release DDC and form $Cu(DDC)_2$ *in situ*. The CuS NP + NIR laser treatment can effectively increase the intra-tumor ROS levels and efficiently activate the DQ prodrug. The CDL therapy kills cancer cells through multiple mechanisms, including ROS amplification cascade and $Cu(DDC)_2$ chemotherapy. NIR light-triggered tumor-specific “nontoxic-to-toxic” transition can significantly improve the specificity of anticancer effects and reduce systemic toxicity. Also, CDL therapy can effectively induce immunogenic cell death (ICD) and has the potential of eliciting antitumor immunity.

Keywords

CuS nanoparticles; Reactive oxygen species (ROS); Disulfiram prodrug; Near-infrared laser; Immunogenic cell death (ICD)

[*]**Corresponding author: Feng Li, PhD**, 720 South Donahue Drive, Auburn, AL, 36849, USA, Tel:334-844-7406, FZL0023@auburn.edu.

SUPPORTING INFORMATION

Additional supporting material is available.

CONFLICT OF INTEREST

The authors declare that there is no conflict of interest.

1. INTRODUCTION

Triple-negative breast cancer (TNBC) is one type of breast cancer missing progesterone, estrogen, and human epidermal growth factor receptor 2 (HER-2) receptors. TNBC is a aggressive tumor with invasive and metastatic properties (Carey et al., 2010; Garrido-Castro et al., 2019). Due to the heterogeneous nature of TNBC, drugs targeting a specific signaling pathway or protein usually cannot achieve satisfactory anticancer efficacy (Nedeljković and Damjanović, 2019). Cytotoxic chemotherapy has been commonly used for TNBC treatment (Carey et al., 2010; Garrido-Castro et al., 2019; Nedeljković and Damjanović, 2019). However, chemotherapy often shows short-term benefits and limited patient survival. The clinical use of chemotherapy is also limited by the toxic side effects and development of drug resistance (Nedeljković and Damjanović, 2019). Thus, there is a great need for novel therapies for TNBC. Recently, cancer immunotherapy, particularly the immune checkpoint inhibitors *(e.g.,* anti-PD1 antibody, anti-PD-L1 antibody), have demonstrated great potential for treating cancer through the induction of anticancer immunity. The immune therapy can effectively treat or prevent cancer metastasis and benefit patients with TNBC which has a high incidence of metastasis. The development of therapeutics to kill cancer cells through immunogenic cell death (ICD) is a promising strategy to elicit antitumor immunity and improve the efficacy of immunotherapy for TNBC (Feng et al., 2020).

Copper sulfide nanoparticle (CuS NP) is a nanomaterial with great potential for biomedical applications (Goel et al., 2014; Zhou et al., 2016). CuS NP has a strong near-infrared (NIR) absorption because of the d-d transition in copper and thus has been utilized for photothermal therapy (PTT) and photodynamic therapy (PDT) against cancer and other diseases (Chen et al., 2015; Chen et al., 2017; Chu et al., 2018; Huang et al., 2017; Qiao et al., 2019; Shi et al., 2018; Zhou et al., 2010). Previous studies have also demonstrated promise of CuS NP for bioimaging applications such as positron emission tomography (Cui et al., 2018; Zhou et al., 2015a; Zhou et al., 2015b) and photoacoustic tomography (Chen et al., 2017; Ku et al., 2012). CuS NP showed excellent biocompatibility and low toxicity. It can be cleared from the body after degradation and alleviate long-term exposure toxicity, which is a concern for the use of NPs made with noble metals (Shi et al., 2019). When treated with NIR laser, CuS NP can efficiently produce ROS through photodynamic effects (Gu et al., 2019). The heat generated through photothermal effects can also activate dissolved oxygen to generate ROS (Li et al., 2017). Cu^{2+} released from CuS NP can also facilitate the production of ROS through Haber-Weiss and Fenton reactions (Dong et al., 2020). These properties of CuS NP can be utilized for cancer therapy by increasing the level of ROS in cancer cells. Cancer cells are more vulnerable than normal cells to ROS-mediated cytotoxicity because they have elevated baseline ROS levels to promote tumor progression and have fewer capacities to maintain redox hemostasis (Perillo et al., 2020).

Disulfiram (DSF) has been used as an anti-alcoholism drug for decades. Also, DSF has copper-dependent anticancer activities (Bruning and Kast, 2014; McMahon et al., 2020; Skrott et al., 2017). DSF is metabolized *in vivo* and converted into DDC. DDC complexes with Cu^{2+} to generate $Cu(DDC)_2$, which induces cancer cell death by targeting p97 segregase adaptor nuclear protein localization protein 4 (NPL4) and inhibiting proteasome protein degradation pathway (Bruning and Kast, 2014; Skrott et al., 2017). DSF has been

tested in several clinical trials for treating castration-resistant prostate cancer, glioblastoma, and breast cancer (https://clinicaltrials.gov). However, the clinical use of DSF did not achieve satisfactory outcomes due to its poor stability in the body, which results inadequate $Cu(DDC)_2$ concentration in the tumor tissue (Zhang et al., 2020). Therefore, novel formulations for DSF-based therapy are needed to obtain sufficient intratumoral $Cu(DDC)_2$ concentration and have potent anticancer efficacy (McMahon et al., 2020; Zhao et al., 2018a). Previously, we prepared the $Cu(DDC)_2$ NP formulation with a stabilized metal ion ligand complex (SMILE) technology developed in our laboratory. The $Cu(DDC)_2$ NP showed excellent anticancer efficacies against breast cancer and prostate cancer in the preclinical setting (Chang et al., 2020; Chen et al., 2018; Huang et al., 2020).

In the current work, we propose to use a novel CDL combination therapy for cancer treatment (Figure 1). The DQ prodrug is stable in the blood and normal tissues but can be activated specifically at the tumor microenvironment with elevated ROS levels to produce DDC. The ROS generated by NIR laser + CuS treatment will enhance the activation of the DQ prodrug. The DDC complexes with Cu^{2+} to form $Cu(DDC)_2$ *in situ* at the tumor site. The CDL therapy kills cancer through multiple mechanisms, including (1) *in situ* formed $Cu(DDC)_2$ chemotherapy, (2) tumor ROS amplification, and (3) the induction of ICD. The CDL combination therapy uses the localized NIR laser to activate DQ prodrug and trigger the nontoxic-to-toxic transition at the tumor site. Since the individual ingredients of CDL combination therapy have low toxicity and excellent biocompatibility, the toxic side effects associated with their exposure in normal tissues/organs will be minimal. The synergistic or additive effects of multiple anticancer mechanisms will effectively kill the cancer cells by targeting multiple pathways and avoid or delay the emergence of acquired resistance. In addition, the induction of ICD will bolster adaptive anticancer immune responses to suppress cancer metastasis and potentially enhance the efficacy of immune checkpoint inhibitors.

2. MATERIAL AND METHODS

2.1 Material

PEG_{2K}-$PLA_{1.8K}$ was synthesized with the ring-opening polymerization method described in our previous study (Li et al., 2010). 2',7'-dichlorodihydrofluorescein diacetate (DCF-DA) was ordered from EMD Millipore Corp (Darmstadt, Germany). Flouroprobe 5,59,6,69-tetrachloro-1,19,3,39-tetraethylbenzimidazol-carbocyanine iodide (JC-1) was ordered from AdipoGen Life Science Inc (San Diego, CA). Propidium iodide (PI) and Calcein-AM were ordered from BD science Inc (San Diego, CA). FITC Annexin V apoptosis detection kit was from BioLegend (San Diego, CA). 3-(4,5-dimethylthiazol-2-yl)-2,5-diphenyl tetrazolium bromide (MTT) was purchased from Swiss Pharmaceutical Company Novartis (Basel, Switzerland). Anti-Calreticulin antibody (ab2907) was purchased from abcam. Oxaliplatin (OXP) was from LC Laboratories. DQ was synthesized as previously reported (Pan et al., 2019) and characterized with ^{1}H-NMR, ESI/MS, and Thin-layer chromatography (TLC). Other supplies were purchased from VWR International, LLC (Radnor, USA). Lewis lung carcinoma (LLC) lung cancer cells, 4T1 and EMT 6 breast cancer cells, as well as 3T3 fibroblast cells were from American Type Culture Collection (ATCC). mCherry-KDEL

over-expression 4T1 cells (4T1-mCherry) were kindly provided by Dr. Brent Johnston at Dalhousie University, Canada (Gebremeskel et al. 2017). The 4T1, EMT6, 3T3 cells were cultured in a humidified atmosphere containing 5% CO_2 at 37 °C using Roswell Park Memorial Institute (RPMI) 1640 with 10% FBS and 1% antibiotic antimycotic. LLC cells were cultured with Dulbecco's Modified Eagle's Medium (DMEM) with with 10% FBS and 1% antibiotic antimycotic.

2.2 Preparation and characterizations of CuS NP

CuS NP was synthesized as previously reported (Zhao et al., 2018b). In brief, bovine serum albumin (BSA, 250 mg) was dissolved in purified water (7.5 mL). $CuCl_2$ solution (100 μL, 0.2 M) was slowly added into the BSA solution at room temperature under stirring. Then, NaOH solution (1 M, 0.5 mL) and Na_2S (0.2 M, 2 mL) were added sequentially. The reaction mixture was heated for 30 minutes at 90 °C to yield CuS NP. The synthesized CuS NP was purified by dialysis against deionized water, freeze-dried, and stored in a refrigerator. CuS NP was observed with transmission electron microscopy (TEM, Zeiss EM10) and analyzed with energy dispersive X-ray spectroscopy (EDS; X-Max detector, Oxford Instruments Inc). The size of CuS NP was determined with dynamic light scattering (DLS; Zetasizer, Malvern). The CuS NP concentration was determined based on the Cu concentration. Briefly, 1 mg CuS NP sample was dissolved with 0.8 mL HNO_3 (0.6 N) and sonicated for 1 hour to dissolve CuS NP. Then, 0.2 mL ammonia was added to the above solution to form Cu $(NH_3)^{2+}$.The Cu concentration was determined by the absorption at 618 nm (Mehlig, 1941; Villanueva et al., 2016). The percentage of CuS content in the NP formulation was calculated using the following formula: Amount of CuS / Total Amount of NPs x 100%. The CuS NP was also analyzed by X-ray powder diffraction (XRD) by using a diffractometer (Bruker, D8 ADVANCE). UV-Vis absorption spectrum of CuS NP was determined with Ultrospec 2100 pro UV/Visible Spectrophotometer. The CuS NP was also analyzed with Fourier-transform infrared spectroscopy (FT-IR) with spectrum in the range of 650-400 cm^{-1}. The serum stability of CuS NP was determined by measuring the change of particle size in phosphate-buffered saline (PBS, pH 7.4) with fetal bovine serum (FBS, 10%). To determine the photothermal effects of CuS NP, the NP samples were treated with NIR laser (808 nm), and the change of temperature was monitored with a digital thermometer. The effects of CuS NP concentration, laser power density, and exposure time on temperature change were determined.

2.3 Preparation and characterizations of DQ micelle

DQ-loaded micelle was prepared with a film-dispersion method (Li et al., 2011). Briefly, DQ (3.5 mg) and PEG-PLA polymer (35 mg) were dissolved with dichloromethane (DCM). Then, DCM was removed with a rotary evaporator to form a thin layer of film. The film was dispersed in 1 mL PBS with sonication, and unloaded drugs were removed with centrifugation at 6,700 rcf for 10 min. The DQ concentration in micelle formulations was determined with a UV-Vis spectrometer at 270 nm. The percentage of DQ content in the micelle formulation was calculated using the following formula: Amount of DQ / Total Amount of DQ and Polymer Carriers x 100%. The critical micelle concentration (CMC) was determined with a pyrene-based method (Li et al., 2010). The size of micelles were determined with DLS (Zetasizer, Malvern). The morphology was determined with

transmission electron microscopy TEM (Zeiss EM10).The serum stability of DQ micelle was determined by measuring the change of particle size in FBS (10%) containing PBS (pH 7.4).

2.4 Anticancer effects on 2D cultured cell line

Cells were seeded into 24-well plates (15,000 cells / well) and incubated overnight. For the CDL combination therapy, CuS NP was incubated with cells for 3 hours prior to NIR laser treatment. Cells were treated with an infrared diode laser (MDL-N-808) with beam diameter of 1.5 cm, intensity of 2.54 W/cm^2 for 5 minutes. Then, DQ micelle was added and incubated for additional 45 hours. Other groups were treated similarly by using proper controls. Cells were treated with the same method with minor adjustments for other assays in this study. At the end of treatment, the cell viability was determined with the MTT assay (Chang et al., 2020). Calcein-AM/PI staining was also performed 24 hours post treatment to test the anticancer effects. Dead and viable cells were observed by the red fluorescence (dead) and the green fluorescence (viable), respectively.

2.5 Anticancer effects on 3D tumor spheroids

We used a liquid overlay method to establish tumor spheroids as deseribed in our previous studies (Chang et al., 2020). Briefly, a 24-well plate was pretreated with agarose gel (1% w/v) and then was seeded with 4T1 cells. The spheroids were formed typically in five day and then treated with various testing formulations for additional 24 hours. Then, the samples were stained with Calcein-AM/PI. Viable cells with green fluorescence and dead cells with red fluorescence and were observed. We also determined the cell viability of tumor spheroids with the CellTiter-Blue cell viability assay. After treating tumor spheroids with different formulations for 56 hours, tumor spheroids were incubated with CellTiter-Blue dye for additional 4 hours, and the fluorescence intensity was measured (EX 560 nm and EM 590 nm).

2.6 Annexin V apoptosis assay

Cells seeded in a 12-well plate (100,000 cells / well) were treated with different formualtions. Twenty-eight hours post-treatment, cell apoptosis was analyzed with FITC Annexin V apoptosis kit following the vendor’s instruction (Biolegend) with flow cytometry (BD Accuri C6 plus).

2.7 Wound-healing assay

We performed the wound-healing assay as described in our previous studies (Kang et al., 2018). Briefly, the 4T1-mCherry cells were seeded in a 24-well plate to form a confluent monolayer. Then, monolayer was scraped with a pipet tip to produce a scratch. Cells were treated with different formulations and the change of scratch was observed.

2.8 Analysis of intracellular ROS

The intracellular ROS was determined with a DCF-DA dye method. Briefly, cells were seeded in a 24-well plate (70,000 cells per well). Cells were incubated with DCF-DA (20 μM) in serum-free medium at 37 °C for 1 hour and then treated with different formulations

for additional 6 hours. The fluorescence intensity was determined (EX 485nm / EM 535nm), and the fluorescence photos were also taken by the cytation 5 cell imaging multi-mode reader.

2.9 Mitochondrial membrane potential (MMP) measurement

JC-1 dye was used to determine the change of MMP. The depolarization of the mitochondrial membrane can be determined by monitoring the shift of JC-1 fluorescence from red to green (Tang et al., 2017). In this study, cells seeded in a 24-well plate were treated with different formulations. After 8 hours, the treated cells were incubated with JC-1 dye (0.1 mg/mL) in serum-free media in the dark for 30 minutes. Then, samples were observed with the cytation 5 multi-mode cell imaging reader.

2.10 Biomarkers of immunogenic cell death (ICD)

Cells were seeded in a 24-well plate (100,000 cells per well), and incubated overnight before use. Then, cells treated with different formulations were analyzed to determine the following ICD biomarkers. **(1) Cell surface Calreticulin (CRT)**: Ten hours post-treatment, cells were collected and incubated with anti-calreticulin antibody (Abcam, ab2907; 1:200) for 60 minutes and treated with the FITC-conjugated secondary antibody for 30 minutes (1:200; Goat Anti-Rabbit IgG, Jackson ImmunoResearch). Then, stained cells were analyzed with flow cytometry (BD Acurri C6) to determine the cell surface CRT. **(2) ATP release**. Cell culture media was collected 12 hours after treatment, the ATP concentration in the conditioned culture media was determined with an ATP bioluminescence detection kit (Promega). **(3) High mobility group box 1 protein (HMGB1)**: Cell culture media was collected 18 hours after treatment, and the HMGB1 in the culture media was determined with an HMGB1 ELISA chemiluminescence kit (Novus Biologicals).

2.11 Determination of $Cu(DDC)_2$ with LC/MS

Cells seeded in a 12-well plate (100,000 cells/well) were treated with CDL for 4 hours, then cell lysate and supernatant were collected and mixed with acetonitrile to precipitate proteins. After centrifugation, the supernatant was collected and analyzed with LC/MS to detect the formation of $Cu(DDC)_2$. The analysis was performed on a UPLC system (Waters,USA) with a quadrupole time-of-flight mass spectrometer and electrospray ionization (ESI) in positive mode using Masslynx software (V4.1). Ten microliters of solutions were injected into a C18 column (Waters BEH C18 2.1 mm x 50 mm, 1.7 μm). The mobile phase (flow rate of 200 μL/min) was composed of solution A (100% water) and solution B (100% acetonitrile) beginning at 50% B, held for 1.5 minutes, then linear ramp to 95% B at 11 min, and return to 50% B at 14 min with 4 minutes of re-equilibration.

2.12 Statistical Analysis

Experiments were performed in triplicate or quadruplicate unless otherwise noted. Results were reported as mean ± standard deviation (SD). The difference between groups was analyzed with the unpaired t-test.

3. RESULTS AND DISCUSSIONS

Preparation and characterization of DQ Micelle and CuS NP

We synthesized DQ with 4-Bromomethylphenylboronic acid pinacol ester and sodium diethyldithiocarbamate as shown in Figure S1 (Pan et al., 2019). The structure of DQ was confirmed with ^{1}H-NMR (Figure S1). The ESI/MS (m/z) of DQ was 366.1727, and the calculated [MH+] was 366.17. The purity of the DQ was confirmed with TLC, and no significant impurity spot was observed. DQ was loaded into the PEG-PLA polymeric micelle as described in our previous paper (Li et al., 2011). The PEG-PLA micelle has a CMC value of 5 x 10^{-3} g/L and a particle size of 32 ± 2 nm (Figure S2). DQ was loaded into the hydrophobic core of micelles (Figure 2A) with a DQ concentration of 2.9 ± 0.3 mg/mL and a percentage of drug content of 7.5 ± 0.7%. The DQ micelle had a size of around 155 ± 8 nm as determined by DLS (Figure 2B). The morphology of the DQ micelle was also observed with TEM (Figure 2C). DQ micelle showed outstanding stability in serum-containing medium, and no significant change of particle size was observed in 56 hours (Figure 2D). CuS NP was synthesized with a reported biomineralization method (Zhao et al., 2018b). When $CuCl_2$ solution was mixed with BSA, a blue color mixture was formed, which was due to the coordination interactions of Cu^{2+} and BSA functional groups *(e.g.,* -SH, -NH_2, -COOH). The color of the mixture turned purple after the addition of NaOH solution, which was used to adjust the pH to alkaline conditions to unfold the tertiary structure of BSA and make more amino acid residues available for stabilizing the CuS NPs. The color of the mixture turned into brick red after adding Na_2S, indicating the formation of CuS. Finally, the color of the mixture turned dark green when the system was heated at 90 °C for 30 minutes to form stable CuS NPs. The synthesized CuS NP was purified by dialysis against deionized water, freeze-dried, and stored in a refrigerator. BSA was used as the stabilizer of CuS NP because of the strong affinity between copper and functional groups of BSA (Figure 2E). The percentage of CuS content in the NP formulation was 19.5 ± 0.3%. CuS NP synthesized with this method had a particle size of 81 ± 7 nm as determined with DLS (Figure 2F). The morphology and size of CuS NP was also determined with the TEM (Figure 2G). CuS NP also demonstrated excellent stability. No significant change of particle size was observed after incubation in the serum-containing medium for 56 hours (Figure 2H). The CuS NP showed strong absorption at 808 nm and around the NIR range (Figure 2I). The synthesized CuS NP was also characterized with EDS (Figure 2J), XRD (Figure 2K), and FT-IR (Figure 2L). The results were consistent with previous reports (Li et al., 2018; Wang et al., 2016; Zhang et al., 2015). We tested the photothermal properties of CuS NP treated with NIR laser (808 nm). The treatment of CuS NP with 808 nm laser can significantly increase the temperature, which was dependent on the CuS NP concentration, laser treatment time and power intensity (Figure S3). When the CuS NP (0.1 mM) were treated with laser (808 nm, power density: 2.54 W/cm^2) the temperature increased with time of exposure, while much less increase of temperature was observed in pure water control (Figure S3A). The incrase of laser power intensity led to the temperature increase in CuS NP group (0.1 mM), while minimal effects were observed in the control pure water group (Figure S3B). Our data also demonstrated that the change of temperature was dependent on the CuS NP concentration. After being exposed to laser (power density: 2.54 W/cm^2) for 5

minutes, the temperature of control water sample was around 28.6°C and the temperature of CuS NP sample (0.1 mM) was about 40°C (Figure S3C).

Anticancer activities of CDL combination therapy

We tested the anticancer effects with 4T1 breast cancer cells. Before testing the anticancer effects of CDL combination therapy, we determined the effects of different individual treatments on the viabilities of 4T1 cancer cells with the MTT assay. The DQ micelle did not show significant cell toxicity when incubated with 4T1 cells for 48 hours at a concentration of up to 2 μM (Figure S4A). The unactivated DQ prodrug showed significantly reduced toxicity than the DSF when used in combination with CuS NPs. DQ (2 μM) and CuS NP (0.1 mM) co-treatment showed minimal effects on 4T1 cells' viability (75.0 ± 5.6%). In contrast, the viability of 4T1 cells co-treated with 0.1 mM CuS NP and 1 μM DSF (equivalent to 2 μM DQ) was reduced to 7.3 ± 0.4% (Figure S4B). In the absence of NIR laser, CuS NP showed minimal effects on 4T1 cell viability when its concentration was less than 0.42 mM (Figure S4C). When co-treated with NIR laser (2.54 W/cm2), CuS NP showed concentration-dependent anticancer activities, and the cell viability was around 60% at the highest CuS NP concentration (0.42 mM). We also determined the effects of different laser intensities on 4T1 cell viability. When 0.1 mM CuS NP was used, the cell viability decreased with increased laser intensities. However, in the absence of CuS NP, the treatment with the same laser intensity did not result in significant change of cell viability (Figure S4D). Although a higher concentration of CuS NP or a higher power of laser will have more potent anticancer effects, we will select a relatively low CuS NP concentration and low laser intensity in the CDL combination therapy, which can improve the safety but can still effectively kill cancer cells through multiple anticancer effects achieved by the CDL combination therapy.

Based on these pilot studies, we moved forward to test the anticancer effects of CDL combination therapy. As demonstrated in Figure 3A, none of the CuS (0.1 mM), DQ (2 μM), Laser (2.54 W/cm2) monotherapy group showed significant cytotoxicity after treatment for 48 hours, and cell viability in these groups 95 ± 4%, 93 ± 7%, and 97 ± 6%, respectively. The [DQ+Laser] showed minimal toxicity and the cell viability in this group was 90 ± 5%. The cell viabilities in [CuS + Laser] and [CuS + DQ] groups were 81 ± 2% and 72 ± 7%, respectively. The CDL combination therapy showed the most potent effects with the cell viability of 29% in this group. We also tested the anticancer efficacy with Calcein-AM/PI staining (Figure 3B and Figure S5). The CuS and DQ groups showed no significant change than negative control. The number of dead cells (red) slightly increased in the [CuS + DQ] and [CuS + Laser] groups, which were associated with a reduced number of living cells (green). The CDL group showed the largest dead cells (red) number and significantly reduced the living cells (green) number. We also tested the anticancer effects with 3D-cultured 4T1 tumor spheroids, which can mimic the tumor microenvironment. After receiving different treatments, the cell viability of tumor spheroids were measured with the CellTiter-Blue cell viability assay (Figure 3C). The CuS treated group did not show significant change in cell viability over the negative control group. Cell viability was slightly decreased in [CuS + Laser] and [CuS + DQ] groups. The CDL group showed the most significant reduction of cell viability among all treatment groups. Tumor spheroids were

also stained with Calcein-AM and PI. The CDL combination therapy group had the most potent anticancer effects, showing the least living cells (green) number and the largest dead cells (red) number among all treatment groups. Both [CuS + DQ] and [CuS + Laser] groups showed more dead cells than the negative control but less than the CDL combination therapy group (Figure 3D). Similar trends were observed in the colony formation study. The CDL treatment showed the most potent effects on the inhibition of the colony formation. The [CuS + Laser] and [CuS + DQ] treatment groups also showed significant inhibition of cell colony but were less effective than the CDL group (Figure 3E). Next, we performed wound-healing studies. This study can evaluate the effects of different treatments on cell metastasis (Chang et al., 2020). The treatment with DQ or CuS alone did not show noticeable inhibition of wound healing. Some minor effects were observed in [CuS + Laser] and [CuS + DQ] groups. The CDL combination therapy group showed the most significant inhibition of wound healing (Figure 4). These results indicated that CDL therapy might inhibit cancer metastasis, which needs to be further confirmed with *in vivo* studies with a metastatic tumor model.

We also tested CDL combination therapy and relevant controls with LLC lung cancer cells and EMT 6 breast cancer cells, as well as 3T3 fibroblast cells. Despite the potent cytoxocity of CDL combination therapy group in these cells, all other control groups showed minimal effects (Figure S6). Although the CDL also showed toxicity towards the 3T3 fibroblast cells, the localized laser treatment for *in vivo* application can trigger the anticancer effects in tumor tissues and avoid toxicity in normal tissues and organs.

Anticancer mechanisms of CDL combination therapy

We hypothesize that the CDL combination therapy kills cancer through $Cu(DDC)_2$ chemotherapy and ROS amplification. To confirm the $Cu(DDC)_2$ formation in cells treated with CDL combination therapy, we analyzed cell samples with LC/MS. The peak at 359 m/z confirmed the formation $Cu(DDC)_2$ after CDL treatment (Figure S7). We also observed the formation of $Cu(DDC)_2$ in the DQ+CuS treated group. Further studies will be need to quantitatively compare the concentration of $Cu(DDC)_2$ in different treatment groups. To further understand the anticancer mechanism, we determined the intracellular ROS levels in 4T1 cells using TNBCH-DA as a ROS detection probe, which shows a green fluorescence at elevated ROS levels. As shown in Figure 5A&B, CDL combination therapy induced the highest ROS level due to the activation of the ROS amplification cascade (Figure 1). [CuS + DQ] and [CuS + Laser] groups also showed significantly elevated ROS levels but were less than the CDL group. A slight increase in ROS levels was observed in the DQ group. There was no significant increase in ROS levels in the CuS group. The intracellular ROS levels in different treatment groups showed a good correlation with the cytotoxicity study results in Figure 3, indicating ROS amplification was one of the anticancer mechanisms for CDL combination therapy.

JC-1 was used in this study to detect the change of the MMP. In normal cells with high MMP, JC-1 forms J-aggregates with red fluorescence. The green fluorescence (J-monomers) increases at the reduced MMP. As shown in Figure 5C & Figure S8, the control, CuS, Laser, DQ, [DQ+Laser] groups showed strong red fluorescence but a negligible green fluorescence,

demonstrating high MMP in these groups. [CuS+Laser], [CuS + DQ], and CDL combination therapy groups showed a significant increase of green fluorescence signals and associated with the decrease of red fluorescence, indicating the reduction of MMP in these groups. Among them, the CDL group showed the most significant decrease in MMP. A previous study reported that the disulfiram/copper combination therapy could disrupt mitochondrial membrane integrity and result in mitochondria-dependent cell apoptosis (Xu et al., 2020; Yang et al., 2016). The CDL combination therapy might have a similar effect and kill cancer cells through the amplified oxidative stress and by the disruption of mitochondrial membranes.

To further investigate cell death patterns, we performed annexin V apoptosis assay (Kang et al., 2017) to determine the percentage of early-stage and late-stage apoptotic cells. The CDL combination therapy group showed 14.8 ± 0.9 % early-stage apoptotic cells and 29 ± 2.1% of late-stage apoptotic cells. The [CuS + laser] group showed 8.7 ± 0.3% early-stage apoptotic cells and 9.5 ± 4.4% of late-stage apoptotic cells. The [CuS + DQ] group showed 10.8 ± 0.7% early-stage apoptotic cells and 17.8 ± 8.4% of late-stage apoptotic cells (Figure 5D). These results indicated that CDL combination therapy could efficiently induce cell apoptosis in cancer cells.

ICD refers to any type of cell death that releases damage-associated molecular patterns (DAMPs) and stimulates anticancer immunity (Zhou et al., 2019). A variety of therapy, including chemotherapy, PDT, PTT, and radiotherapy (RT), can efficiently induce ICD and generate "*in situ* tumor vaccines" to convert a "cold" tumor immune microenvironment (TIME) to a "hot" one, providing a new approach of cancer therapy. Cells undergoing ICD were often characterized by three biomarkers: (1) Cell-surface translocation of CRT; (2) ATP release; and (3) HMGB1 release (Galluzzi et al., 2020). CRT transfers to the cell surface and can act as the "eat-me" signal to antigen-presenting cells (APCs) with CD91 receptors. Extracellular ATP acts as a short-range "find-me" signal. HMGB1 is a biomarker of late-stage ICD. The released extracellular HMGB1 is needed for antigen presentation by dendritic cells (DCs). DAMPs facilitate the presentation of antigen released from cancer cells, activate anticancer cytotoxic T cells, and establish long-term adaptive anticancer immunity. The induction of ICD can activate anticancer immunity and enhance the anticancer efficacy of immunotherapy, such as immune checkpoint inhibitors (Kepp and Kroemer, 2020). Various ICD inducers have been explored in previous studies (Serrano-del Valle et al., 2019). Despite their different action mechanisms, two common features were often observed and played a central role in driving ICD: ER stress and elevated ROS levels (Serrano-del Valle et al., 2019). Previous studies with disulfiram/Cu therapy and our unpublished data with $Cu(DDC)_2$ NP showed the induction of ICD in colorectal and breast cancer cells (Sun et al., 2020; You et al., 2019). $Cu(DDC)_2$ can inhibit proteasome-mediated protein degradation, cause accumulation of misfolded proteins in the endoplasmic reticulum (ER), induce ER stress, and trigger the exposure of danger signals (Serrano-del Valle et al., 2019). Bortezomib, a proteasome inhibitor that inhibits protein degradation, can also function as an efficient ICD inducer (Serrano-del Valle et al., 2019). Furthermore, both PDT and PTT can effectively induce ICD due to their effects on ER stress and ROS generation (Duan et al., 2019). Therefore, we hypothesize that the CDL combination therapy could efficiently induce ICD. To test this hypothesis, we determined the ICD biomarkers in 4T1

cells treated with CDL therapy (Figure 6). The cell surface translocation of CRT was determined with flow cytometry after staining cells with anti-CRT primary antibody and fluorescence-labeled secondary antibody (Figure 6A). The CDL therapy group showed the highest level of cell surface CRT. There was a slight increase of cell surface CRT in [CuS + Laser] and [CuS + DQ] groups compared to the negative control. The treatment with [DQ + Laser] and other monotherapy did not result in significant increase of cell surface CRT. The CDL treatment showed a similar level of cell surface CRT levels as compared to the OXP treated group (positive control). The released ATP in the cell culture medium was determined (Figure 6B). The results demonstrated that CDL therapy resulted in the most significant ATP release. The [CuS + Laser] and [CuS + DQ] treatment also resulted in significant increase of extracellular ATP in cell culture medium. There was no substantial change of extracellular ATP in CuS group compared with the control group. Further, we determined the released HMGB1 in conditioned cell culture medium using ELISA (Figure 6C). The CDL combination therapy significantly increased the release of HMGB1. [CuS + Laser] and [CuS + DQ] treatment also increased the release of HMGB1 when compared with the negative control group. However, the CuS group had a similar level of HMGB1 release as the control group. These studies indicate that the treatment of cells with CDL combination therapy could induce ICD and activate anticancer immunity. The CDL therapy kill the cancer through $Cu(DDC)_2$ chemotherapy and elevated intracellular ROS levels. Both $Cu(DDC)_2$ and ROS induce ER stress and result in ICD (Deng et al., 2020). Accordingly to the definition of type I or type II ICD inducer described in a previous paper (Garg et al., 2015), the CDL therapy works as type II inducer. However, further studies might be need to confirm whether it is a type I or type II inducer.

In this study, we developed a novel CDL combination therapy for cancer treatment. It is superior to previously reported disulfiram-based therapies due to its innovative features (McMahon et al., 2020; Tang et al., 2020). The CDL therapy kills cancers through multiple mechanisms, including *in situ* formed $Cu(DDC)_2$ chemotherapy, intratumoral ROS amplification, and induction of ICD. **(1)** NIR laser plus CuS NP treatment can elevate ROS levels in tumor tissues due to photodynamic effects. **(2)** ROS-responsive DQ prodrug can be selectively activated at the tumor site in response to elevated ROS levels to release DDC. DDC complexes with Cu^{2+} to produce anticancer $Cu(DDC)_2$ *in situ* at the tumor site. DQ is stable and has a minimal release of DDC at normal tissues/organs with low ROS levels. The activated DQ will further increase the ROS levels in tumor cells through ROS amplification cascade. **(3)** CuS NP will function as the Cu^{2+} reservoir and release Cu^{2+} in response to NIR laser-induced CuS NP degradation. **(4)** DDC and Cu^{2+} form $Cu(DDC)_2$ complex *in situ* at the tumor site, which induces cell death and proteotoxic stress by targeting P97 segregase adaptor NPL4 (Skrott et al., 2017). **(5)** Both $Cu(DDC)_2$ chemotherapy and elevated ROS can induce ICD in cancer cells and activate the anticancer immune responses. It will not only kill primary tumors but also prevent or treat metastatic ones.

In the current study, CuS NP was used to trigger the ROS generation in response to NIR light treatment and function as a source of Cu^{2+} to form $Cu(DDC)_2$ complex for chemotherapy. A recent study showed that nanoscale copper coordination polymers can enhance the induction of ICD through the Cu^{+} triggered hydroxyl radical production and

Cu^{2+} mediated elimination of GSH (Wang et al., 2021). This mechanism might also contribute to the anticancer effects of our CDL combination therapy and is worthwhile to be investigated in future studies. Moreover, the potential of CDL therapy for induction of ICD was determined in the current study based on *in vitro* cell-based assays. It is critical to perform *in vivo* pre-clinical studies to test the CDL therapy for its anticancer efficacy and potential for anticancer immune therapy in future studies. The CDL therapy can potentially convert a "cold" TIME into a "hot" TIME and thus enhance the efficacy of anti-PD-L1 antibody and other immune checkpoint inhibitors. Future investigation of the immunopotentiating property of CDL therapy is warranted.

4. CONCLUSION

In this study, we developed a CDL combination therapy as a novel therapeutic approach for treating TNBC. The CDL combination therapy can enhance anticancer efficacy due to the combination of multiple anticancer mechanisms, including $Cu(DDC)_2$ chemotherapy and oxidative stress amplification. This therapy will have minimal toxic side effects due to tumor-specific NIR light-activated "nontoxic-to-toxic" transition. Because of its unique mechanism of action, the CDL combination therapy can be used as a broad-spectrum anticancer therapy for different cancers. Cancer cells with elevated ROS levels will be more sensitive to CDL therapy. In addition, the CDL therapy will also have the potential to enhance the anticancer efficacy through eliciting antitumor immunity.

Supplementary Material

Refer to Web version on PubMed Central for supplementary material.

ACKNOWLEDGEMENT

This work was financially supported by the following resources: Launch Innovation Award (F, Li), Auburn University start-up fund (F. Li), NIH MIRA R35GM133795 (R Chen). We thank Dr. Melissa Boersma at Auburn University Mass Spectrometry Center for LC/MS analysis.

5. DATA AVAILABILITY

The data of this study is available from the corresponding authors on reasonable request.

REFERENCES

Bruning A, Kast RE, 2014. Oxidizing to death: disulfiram for cancer cell killing. Cell Cycle 13, 1513–1514. [PubMed: 24759086]

Carey L, Winer E, Viale G, Cameron D, Gianni L, 2010. Triple-negative breast cancer: disease entity or title of convenience? Nature reviews Clinical oncology 7, 683–692.

Chang Y, Jiang J, Chen W, Yang W, Chen L, Chen P, Shen J, Qian S, Zhou T, Wu L, Hong L, Huang Y, Li F, 2020. Biomimetic metal-organic nanoparticles prepared with a 3D-printed microfluidic device as a novel formulation for disulfiram-based therapy against breast cancer. Applied Materials Today 18, 100492.

Chen F, Hong H, Goel S, Graves SA, Orbay H, Ehlerding EB, Shi S, Theuer CP, Nickles RJ, Cai W, 2015. In vivo tumor vasculature targeting of CuS@ MSN based theranostic nanomedicine. ACS nano 9, 3926–3934. [PubMed: 25843647]

Chen G, Ma B, Wang Y, Xie R, Li C, Dou K, Gong S, 2017. CuS-Based Theranostic Micelles for NIR-Controlled Combination Chemotherapy and Photothermal Therapy and Photoacoustic Imaging. ACS Applied Materials & Interfaces 9, 41700–41711. [PubMed: 29154532]

Chen W, Yang W, Chen P, Huang Y, Li F, 2018. Disulfiram Copper Nanoparticles Prepared with a Stabilized Metal Ion Ligand Complex Method for Treating Drug-Resistant Prostate Cancers. ACS Applied Materials & Interfaces 10, 41118–41128. [PubMed: 30444340]

Chu Z, Wang Z, Chen L, Wang X, Huang C, Cui M, Yang D-P, Jia N, 2018. Combining Magnetic Resonance Imaging with Photothermal Therapy of CuS@BSA Nanoparticles for Cancer Theranostics. ACS Applied Nano Materials 1, 2332–2340.

Cui L, Xiong C, Zhou M, Shi S, Chow DS, Li C, 2018. Integrin αvβ-Targeted [(64)Cu]CuS Nanoparticles for PET/CT Imaging and Photothermal Ablation Therapy. Bioconjug Chem 29, 4062–4071. [PubMed: 30404438]

Deng H, Zhou Z, Yang W, Lin L.-s., Wang S, Niu G, Song J, Chen X, 2020. Endoplasmic Reticulum Targeting to Amplify Immunogenic Cell Death for Cancer Immunotherapy. Nano Letters 20, 1928–1933. [PubMed: 32073871]

Dong C, Feng W, Xu W, Yu L, Xiang H, Chen Y, Zhou J, 2020. The Coppery Age: Copper (Cu)-Involved Nanotheranostics. Advanced Science 7, 2001549. [PubMed: 33173728]

Duan X, Chan C, Lin W, 2019. Nanoparticle-Mediated Immunogenic Cell Death Enables and Potentiates Cancer Immunotherapy. Angew Chem Int Ed Engl 58, 670–680. [PubMed: 30016571]

Feng B, Niu Z, Hou B, Zhou L, Li Y, Yu H, 2020. Enhancing Triple Negative Breast Cancer Immunotherapy by ICG-Templated Self-Assembly of Paclitaxel Nanoparticles. Advanced Functional Materials 30, 1906605.

Galluzzi L, Vitale I, Warren S, Adjemian S, Agostinis P, Martinez AB, Chan TA, Coukos G, Demaria S, Deutsch E, Draganov D, Edelson RL, Formenti SC, Fucikova J, Gabriele L, Gaipl US, Gameiro SR, Garg AD, Golden E, Han J, Harrington KJ, Hemminki A, Hodge JW, Hossain DMS, Illidge T, Karin M, Kaufman HL, Kepp O, Kroemer G, Lasarte JJ, Loi S, Lotze MT, Manic G, Merghoub T, Melcher AA, Mossman KL, Prosper F, Rekdal Ø, Rescigno M, Riganti C, Sistigu A, Smyth MJ, Spisek R, Stagg J, Strauss BE, Tang D, Tatsuno K, van Gool, SW, Vandenabeele p., Yamazaki T, Zamarin D, Zitvogel L, Cesano A, Marincola FM, 2020. Consensus guidelines for the definition, detection and interpretation of immunogenic cell death. Journal for immunotherapy of cancer 8, e000337. [PubMed: 32209603]

Garg AD, Dudek-Peric AM, Romano E, Agostinis P, 2015. Immunogenic cell death. Int J Dev Biol 59, 131–140. [PubMed: 26374534]

Garrido-Castro AC, Lin NU, Polyak K, 2019. Insights into molecular classifications of triple-negative breast cancer: improving patient selection for treatment. Cancer Discov 9, 176–198. [PubMed: 30679171]

Gebremeskel S, Lobert L, Tanner K, Walker B, Oliphant T, Clarke LE, Dellaire G, Johnston B, 2017. Natural Killer T-cell Immunotherapy in Combination with Chemotherapy-Induced Immunogenic Cell Death Targets Metastatic Breast Cancer. Cancer immunology research 5, 1086–1097. [PubMed: 29054890]

Goel S, Chen F, Cai W, 2014. Synthesis and biomedical applications of copper sulfide nanoparticles: from sensors to theranostics. Small 10, 631–645. [PubMed: 24106015]

Gu X, Qiu Y, Lin M, Cui K, Chen G, Chen Y, Fan C, Zhang Y, Xu L, Chen H, Wan J-B, Lu W, Xiao Z, 2019. CuS Nanoparticles as a Photodynamic Nanoswitch for Abrogating Bypass Signaling To Overcome Gefitinib Resistance. Nano Letters 19, 3344–3352. [PubMed: 30974946]

Huang C-H, Chen P, Liu XM, Li F, 2020. Metal–Organic Nanomaterials for Drug Delivery, Polymers in Therapeutic Delivery. American Chemical Society, pp. 79–95.

Huang J, Zhou J, Zhuang J, Gao H, Huang D, Wang L, Wu W, Li Q, Yang D-P, Han M-Y, 2017. Strong Near-Infrared Absorbing and Biocompatible CuS Nanoparticles for Rapid and Efficient Photothermal Ablation of Gram-Positive and -Negative Bacteria. ACS Applied Materials & Interfaces 9, 36606–36614. [PubMed: 28976189]

Kang X-J, Wang H-Y, Peng H-G, Chen B-F, Zhang W-Y, Wu A-H, Xu Q, Huang Y-Z, 2017. Codelivery of dihydroartemisinin and doxorubicin in mannosylated liposomes for drug-resistant colon cancer therapy. Acta Pharmacol Sin 38, 885–896. [PubMed: 28479604]

Kang X, Zheng Z, Liu Z, Wang H, Zhao Y, Zhang W, Shi M, He Y, Cao Y, Xu Q, 2018. Liposomal codelivery of doxorubicin and andrographolide inhibits breast cancer growth and metastasis. Molecular pharmaceutics 15, 1618–1626. [PubMed: 29498868]

Kepp O, Kroemer G, 2020. A novel platinum-based chemotherapeutic inducing immunogenic cell death. Oncoimmunology 9, 1729022–1729022. [PubMed: 32117595]

Ku G, Zhou M, Song S, Huang Q, Hazle J, Li C, 2012. Copper Sulfide Nanoparticles As a New Class of Photoacoustic Contrast Agent for Deep Tissue Imaging at 1064 nm. ACS Nano 6, 7489–7496. [PubMed: 22812694]

Li B, Jiang Z, Xie D, Wang Y, Lao X, 2018. Cetuximab-modified CuS nanoparticles integrating near-infrared-II-responsive photothermal therapy and anti-vessel treatment. International journal of nanomedicine 13, 7289–7302. [PubMed: 30510418]

Li F, Danquah M, Mahato RI, 2010. Synthesis and Characterization of Amphiphilic Lipopolymers for Micellar Drug Delivery. Biomacromolecules 11, 2610–2620. [PubMed: 20804201]

Li F, Danquah M, Singh S, Wu H, Mahato RI, 2011. Paclitaxel-and lapatinib-loaded lipopolymer micelles overcome multidrug resistance in prostate cancer. Drug delivery and translational research 1, 420–428. [PubMed: 25786362]

Li L, Rashidi LH, Yao M, Ma L, Chen L, Zhang J, Zhang Y, Chen W, 2017. CuS nanoagents for photodynamic and photothermal therapies: Phenomena and possible mechanisms. Photodiagnosis and photodynamic therapy 19, 5–14. [PubMed: 28389371]

McMahon A, Chen W, Li F, 2020. Old wine in new bottles: Advanced drug delivery systems for disulfiram-based cancer therapy. J Control Release 319, 352–359. [PubMed: 31911155]

Mehlig J, 1941. Colorimetric determination of copper with ammonia. Industrial & Engineering Chemistry Analytical Edition 13, 533–535.

Nedeljković M, Damjanović A, 2019. Mechanisms of Chemotherapy Resistance in Triple-Negative Breast Cancer-How We Can Rise to the Challenge. Cells 8, 957.

Pan Q, Zhang B, Peng X, Wan S, Luo K, Gao W, Pu Y, He B, 2019. A dithiocarbamate-based H2O2-responsive prodrug for combinational chemotherapy and oxidative stress amplification therapy. Chemical Communications 55, 13896–13899. [PubMed: 31675022]

Perillo B, Di Donato M, Pezone A, Di Zazzo E, Giovannelli P, Galasso G, Castoria G, Migliaccio A, 2020. ROS in cancer therapy: the bright side of the moon. Experimental & Molecular Medicine, 1–12. [PubMed: 31915368]

Qiao Y, Ping Y, Zhang H, Zhou B, Liu F, Yu Y, Xie T, Li W, Zhong D, Zhang Y, Yao K, Santos HA, Zhou M, 2019. Laser-Activatable CuS Nanodots to Treat Multidrug-Resistant Bacteria and Release Copper Ion to Accelerate Healing of Infected Chronic Nonhealing Wounds. ACS Applied Materials & Interfaces 11, 3809–3822. [PubMed: 30605311]

Serrano-del Valle A, Anel A, Naval J, Marzo I, 2019. Immunogenic Cell Death and Immunotherapy of Multiple Myeloma. Frontiers in Cell and Developmental Biology 7. [PubMed: 30778386]

Shi H, Yan R, Wu L, Sun Y, Liu S, Zhou Z, He J, Ye D, 2018. Tumor-targeting CuS nanoparticles for multimodal imaging and guided photothermal therapy of lymph node metastasis. Acta Biomater 72, 256–265. [PubMed: 29588255]

Shi S, Wen X, Li T, Wen X, Cao Q, Liu X, Liu Y, Pagel MD, Li C, 2019. Thermosensitive Biodegradable Copper Sulfide Nanoparticles for Real-Time Multispectral Optoacoustic Tomography. ACS Applied Bio Materials 2, 3203–3211.

Skrott Z, Mistrik M, Andersen KK, Friis S, Majera D, Gursky J, Ozdian T, Bartkova J, Turi Z, Moudry P, Kraus M, Michalova M, Vaclavkova J, Dzubak P, Vrobel I, Pouckova P, Sedlacek J, Miklovicova A, Kutt A, Li J, Mattova J, Driessen C, Dou QP, Olsen J, Hajduch M, Cvek B, Deshaies RJ, Bartek J, 2017. Alcohol-abuse drug disulfiram targets cancer via p97 segregase adaptor NPL4. Nature 552, 194–199. [PubMed: 29211715]

Sun T, Yang W, Toprani SM, Guo W, He L, DeLeo AB, Ferrone S, Zhang G, Wang E, Lin Z, Hu P, Wang X, 2020. Induction of immunogenic cell death in radiation-resistant breast cancer stem cells by repurposing anti-alcoholism drug disulfiram. Cell Communication and Signaling 18, 36. [PubMed: 32138738]

Tang HX, Liu CG, Zhang JT, Zheng X, Yang DY, Kankala RK, Wang SB, Chen AZ, 2020. Biodegradable Quantum Composites for Synergistic Photothermal Therapy and Copper-Enhanced Chemotherapy. ACS Appl Mater Interfaces 12, 47289–47298. [PubMed: 32975929]

Tang Y, Liang J, Wu A, Chen Y, Zhao P, Lin T, Zhang M, Xu Q, Wang J, Huang Y, 2017. Co-Delivery of Trichosanthin and Albendazole by Nano-Self-Assembly for Overcoming Tumor Multidrug-Resistance and Metastasis. ACS Appl Mater Interfaces 9, 26648–26664. [PubMed: 28741923]

Villanueva ME, Diez A.M.a.d.R., González JA, Pérez CJ, Orrego M, Piehl L, Teves S, Copello GJ, 2016. Antimicrobial activity of starch hydrogel incorporated with copper nanoparticles. ACS applied materials & interfaces 8, 16280–16288. [PubMed: 27295333]

Wang Y, Ding Y, Yao D, Dong H, Ji C, Wu J, Hu Y, Yuan A, 2021. Copper-Based Nanoscale Coordination Polymers Augmented Tumor Radioimmunotherapy for Immunogenic Cell Death Induction and T-Cell Infiltration. Small 17, 2006231.

Wang Z, Huang P, Jacobson O, Wang Z, Liu Y, Lin L, Lin J, Lu N, Zhang H, Tian R, Niu G, Liu G, Chen X, 2016. Biomineralization-Inspired Synthesis of Copper Sulfide–Ferritin Nanocages as Cancer Theranostics. ACS Nano 10, 3453–3460. [PubMed: 26871955]

Xu Y, Zhou Q, Feng X, Dai Y, Jiang Y, Jiang W, Liu X, Xing X, Wang Y, Ni Y, 2020. Disulfiram/copper markedly induced myeloma cell apoptosis through activation of JNK and intrinsic and extrinsic apoptosis pathways. Biomedicine & Pharmacotherapy 126, 110048. [PubMed: 32145587]

Yang Y, Zhang K, Wang Y, Li M, Sun X, Liang Z, Wang L, Chen L, Yang H, Zhu L, 2016. Disulfiram chelated with copper promotes apoptosis in human breast cancer cells by impairing the mitochondria functions. Scanning 38, 825–836. [PubMed: 27353661]

You SY, Rui W, Chen ST, Chen HC, Liu XW, Huang J, Chen HY, 2019. Process of immunogenic cell death caused by disulfiram as the anti-colorectal cancer candidate. Biochem Biophys Res Commun 513, 891–897. [PubMed: 31003768]

Zhang C, Fu Y-Y, Zhang X, Yu C, Zhao Y, Sun S-K, 2015. BSA-directed synthesis of CuS nanoparticles as a biocompatible photothermal agent for tumor ablation in vivo. Dalton Transactions 44, 13112–13118. [PubMed: 26106950]

Zhang T, Kephart J, Bronson E, Anand M, Daly C, Spasojevic I, Berg H, James OG, Healy P, Halabi S, Harrison MR, Armstrong AJ, George DJ, 2020. Disulfiram (DSF) pharmacokinetics (PK) and copper PET imaging in a phase Ib study of intravenous (IV) copper loading with oral DSF for patients with metastatic castration-resistant prostate cancer (mCRPC). Journal of Clinical Oncology 38, 96–96.

Zhao P, Wang Y, Kang X, Wu A, Yin W, Tang Y, Wang J, Zhang M, Duan Y, Huang Y, 2018a. Dual-targeting biomimetic delivery for anti-glioma activity via remodeling the tumor microenvironment and directing macrophage-mediated immunotherapy. Chemical Science 9, 2674–2689. [PubMed: 29732051]

Zhao Y, Cai Q, Qi W, Jia Y, Xiong T, Fan Z, Liu S, Yang J, Li N, Chang B, 2018b. BSA-CuS Nanoparticles for Photothermal Therapy of Diabetic Wound Infection In Vivo. ChemistrySelect 3, 9510–9516.

Zhou J, Wang G, Chen Y, Wang H, Hua Y, Cai Z, 2019. Immunogenic cell death in cancer therapy: Present and emerging inducers. Journal of cellular and molecular medicine 23, 4854–4865. [PubMed: 31210425]

Zhou M, Li J, Liang S, Sood AK, Liang D, Li C, 2015a. CuS Nanodots with Ultrahigh Efficient Renal Clearance for Positron Emission Tomography Imaging and Image-Guided Photothermal Therapy. ACS Nano 9, 7085–7096. [PubMed: 26098195]

Zhou M, Song S, Zhao J, Tian M, Li C, 2015b. Theranostic CuS nanoparticles targeting folate receptors for PET image-guided photothermal therapy. Journal of Materials Chemistry B 3, 8939–8948. [PubMed: 27725882]

Zhou M, Tian M, Li C, 2016. Copper-Based Nanomaterials for Cancer Imaging and Therapy. Bioconjugate Chemistry 27, 1188–1199. [PubMed: 27094828]

Zhou M, Zhang R, Huang M, Lu W, Song S, Melancon MP, Tian M, Liang D, Li C, 2010. A chelator-free multifunctional [64Cu] CuS nanoparticle platform for simultaneous micro-PET/CT imaging

and photothermal ablation therapy. Journal of the American Chemical Society 132, 15351–15358. [PubMed: 20942456]

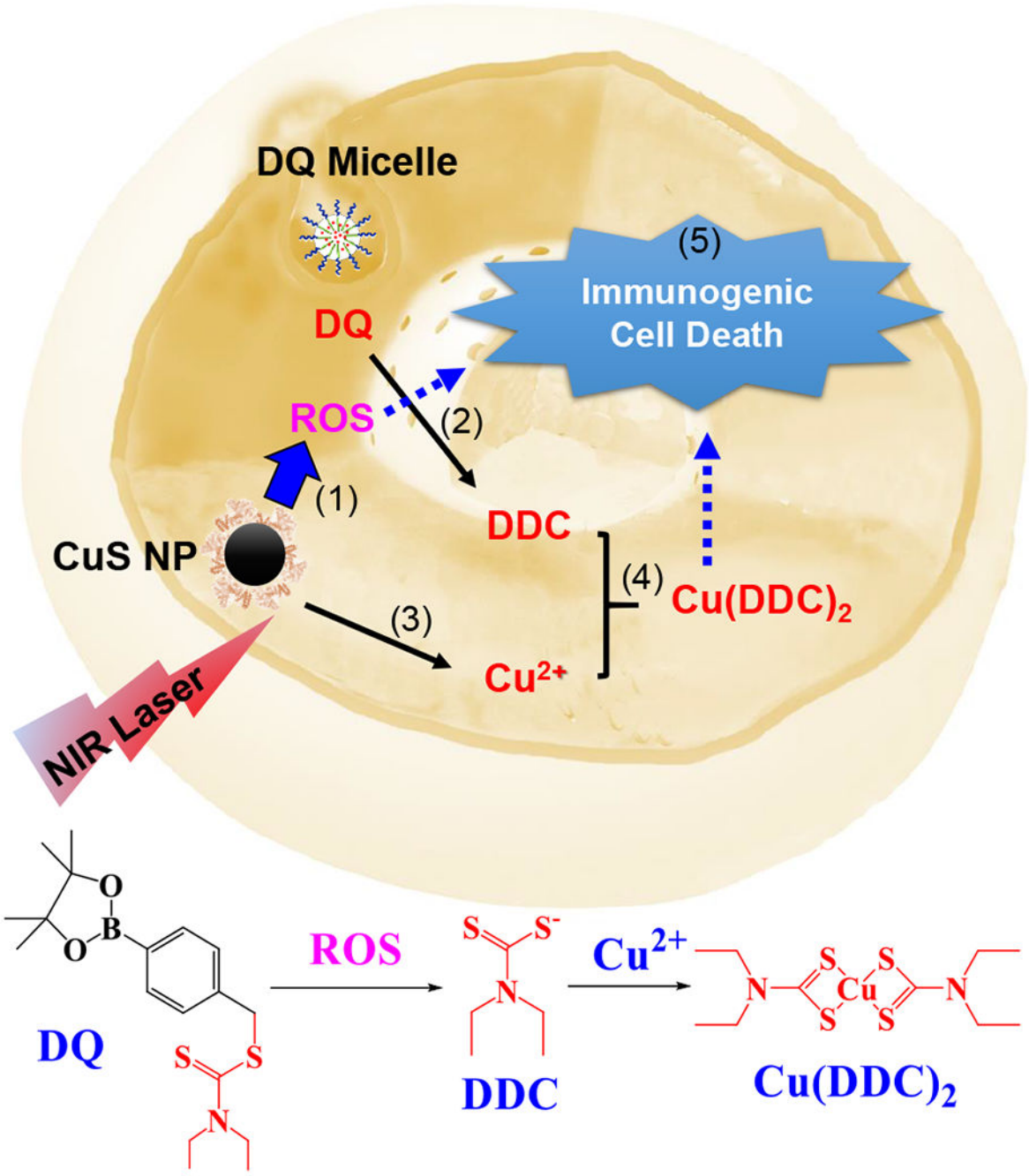

Figure 1. Mechanism of CDL Combination Therapy.

(1) NIR laser + CuS NP treatment increases intracellular ROS. **(2)** ROS converts DQ prodrug to DDC. **(3)** CuS NP release Cu^{2+}. **(4)** DDC and Cu^{2+} form $Cu(DDC)_2$ active anticancer complex. **(5)** $Cu(DDC)_2$ chemotherapy and ROS induce immunogenic cell death in cancer cells.

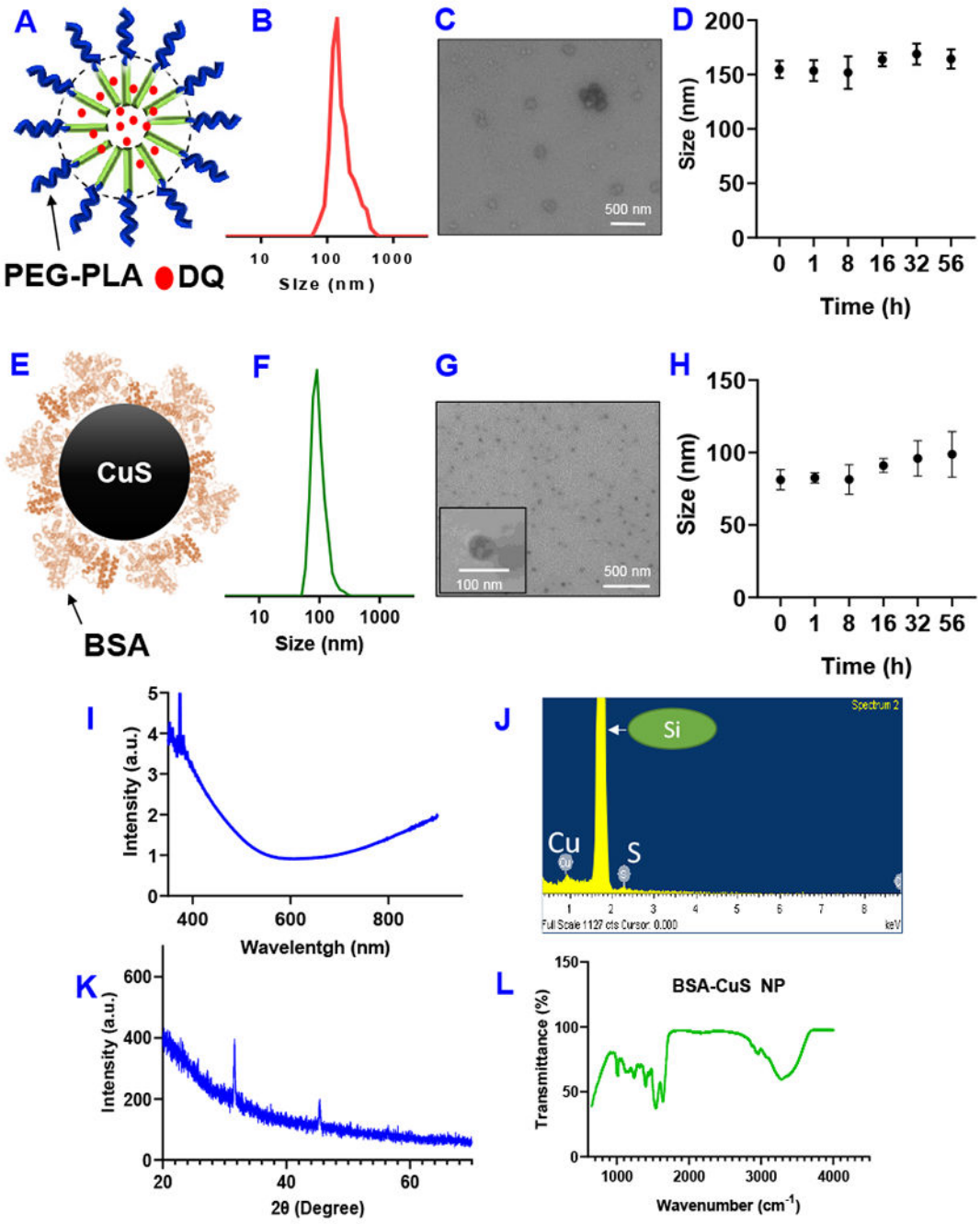

Figure 2.

(A) Schematic representation DQ micelle. **(B)** Particle size of DQ micelle. (**C**) Transmission electron micrograph (TEM) of DQ micelle. (**D**) Stability of DQ micelle in PBS containing serum as determined by the change of particle size. Data are presented as the mean ± SD, n=3. (**E**) Schematic representation of CuS NP. (**F**) Particle size of CuS NP. (**G**) TEM of CuS NP. (**H**) Stability of CuS NP in PBS containing serum as determined by the change of particle size. Data are presented as the mean ± SD, n=3. **(I)** UV–vis absorbance spectrum of CuS NP (1mg/mL). **(J)** Energy dispersive spectrometer (EDS) analysis of CuS NP sample

shows peaks of Cu and S. **(K)** X-ray diffraction (XRD) spectra of CuS NP. **(L)** FT-IR spectra of CuS NP.

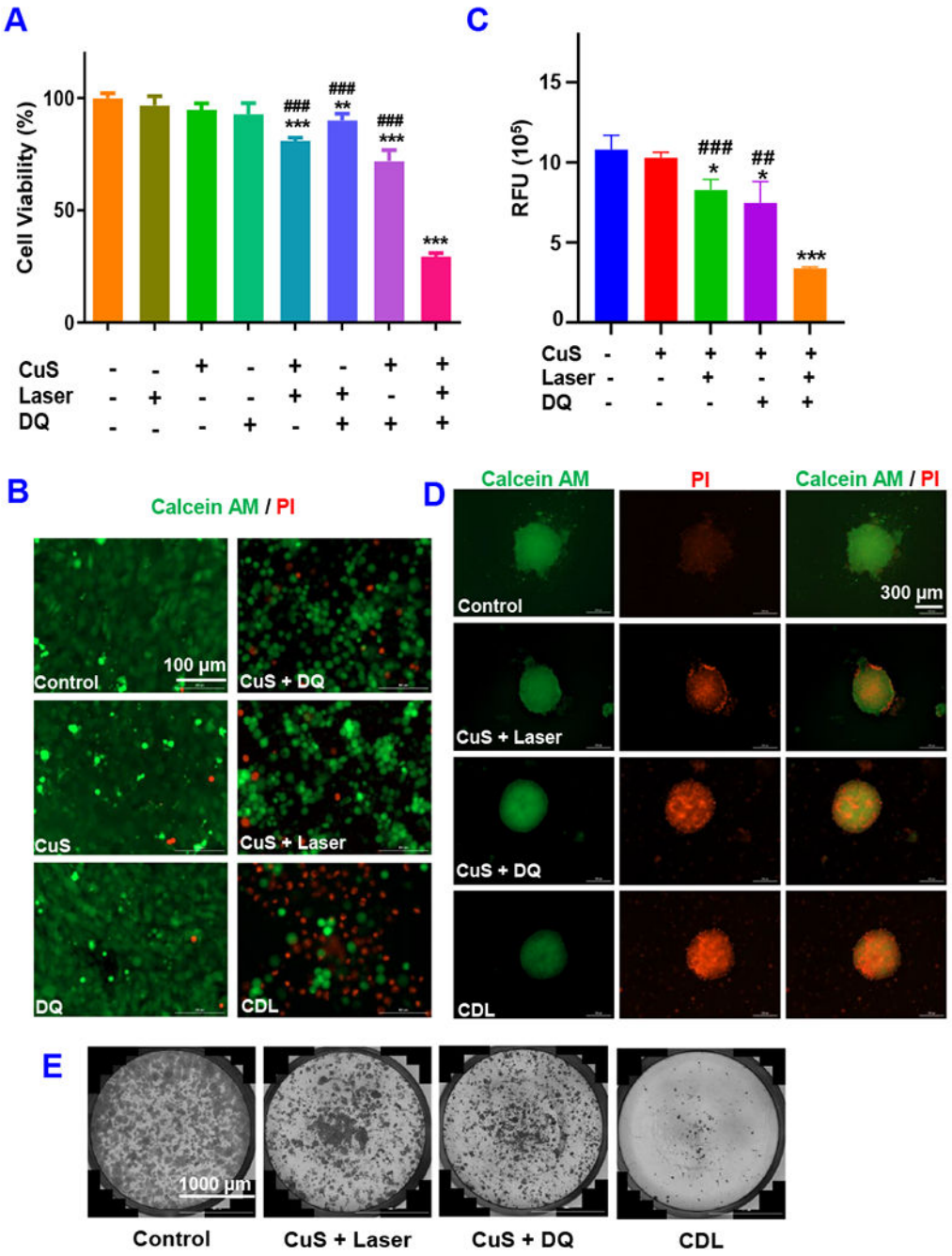

Figure 3. ***In Vitro*** **Antitumor Effects.**

(**A**) the MTT assay and (**B**) Calcein-AM/PI straining. The 4T1 tumor spheroid viability was determined with (**C**) CellTiter-Blue assay and (**D**) Calcein-AM/PI straining. (**E**) Cell colony formation assay. (CuS, 0.1 mM; DQ, 2 μM Laser, 2.54 W/cm^2 for 5 minutes. Data are presented as the mean ± SD, n = 3, * P < 0.05, ** P < 0.01, *** P < 0.001 compared with the negative control group; # # P < 0.01, # # # P < 0.001, compared with CDL treatment group).

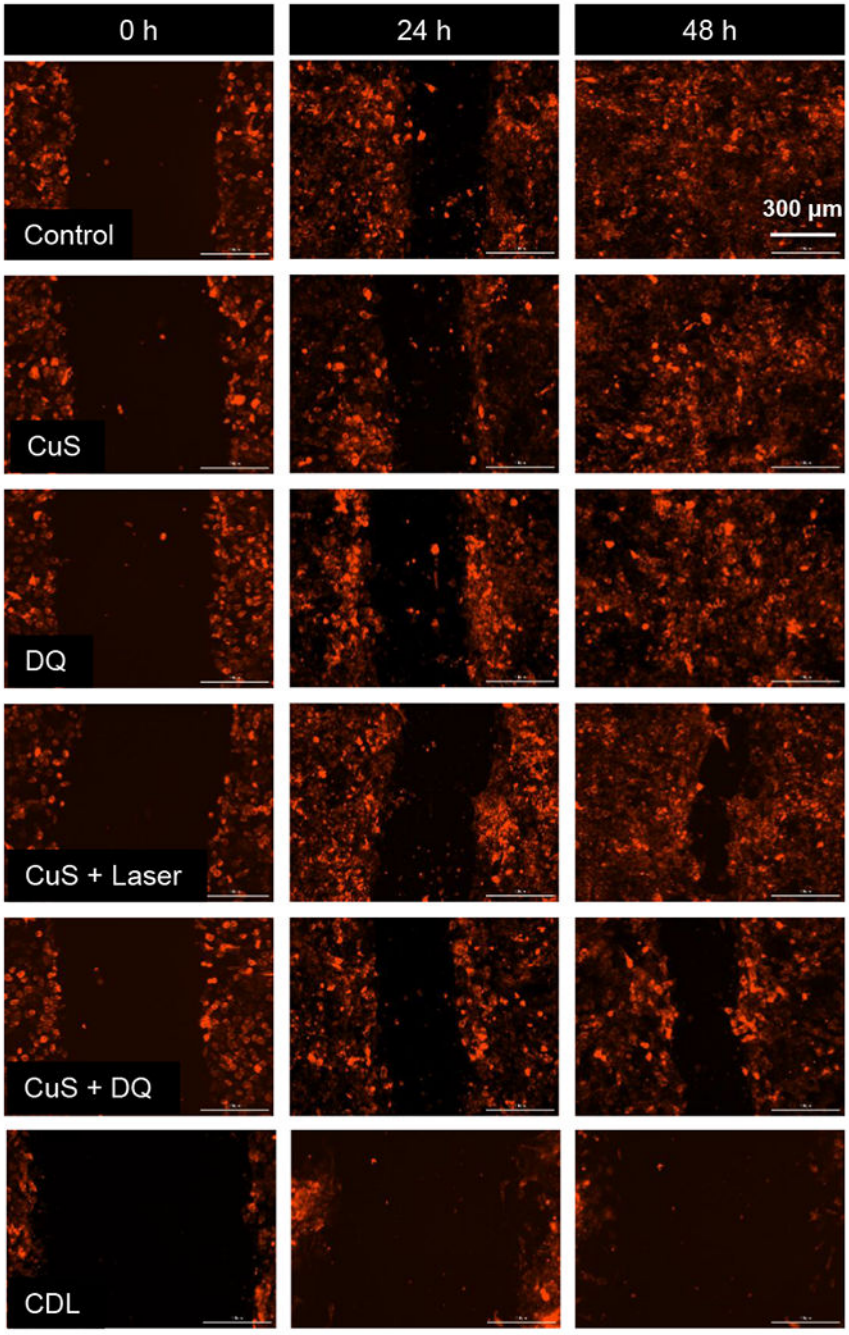

Figure 4. Wound-healing study.

Cells received different treatments after the generation of the scratch. Then, photos were taken at 24 hours and 48 hours. mCherry red fluoresce protein labeled 4T1 cells was used in this study. (CuS, 0.1 mM; DQ, 2 μM; Laser, 2.54 W/cm^2 for 5 minutes.)

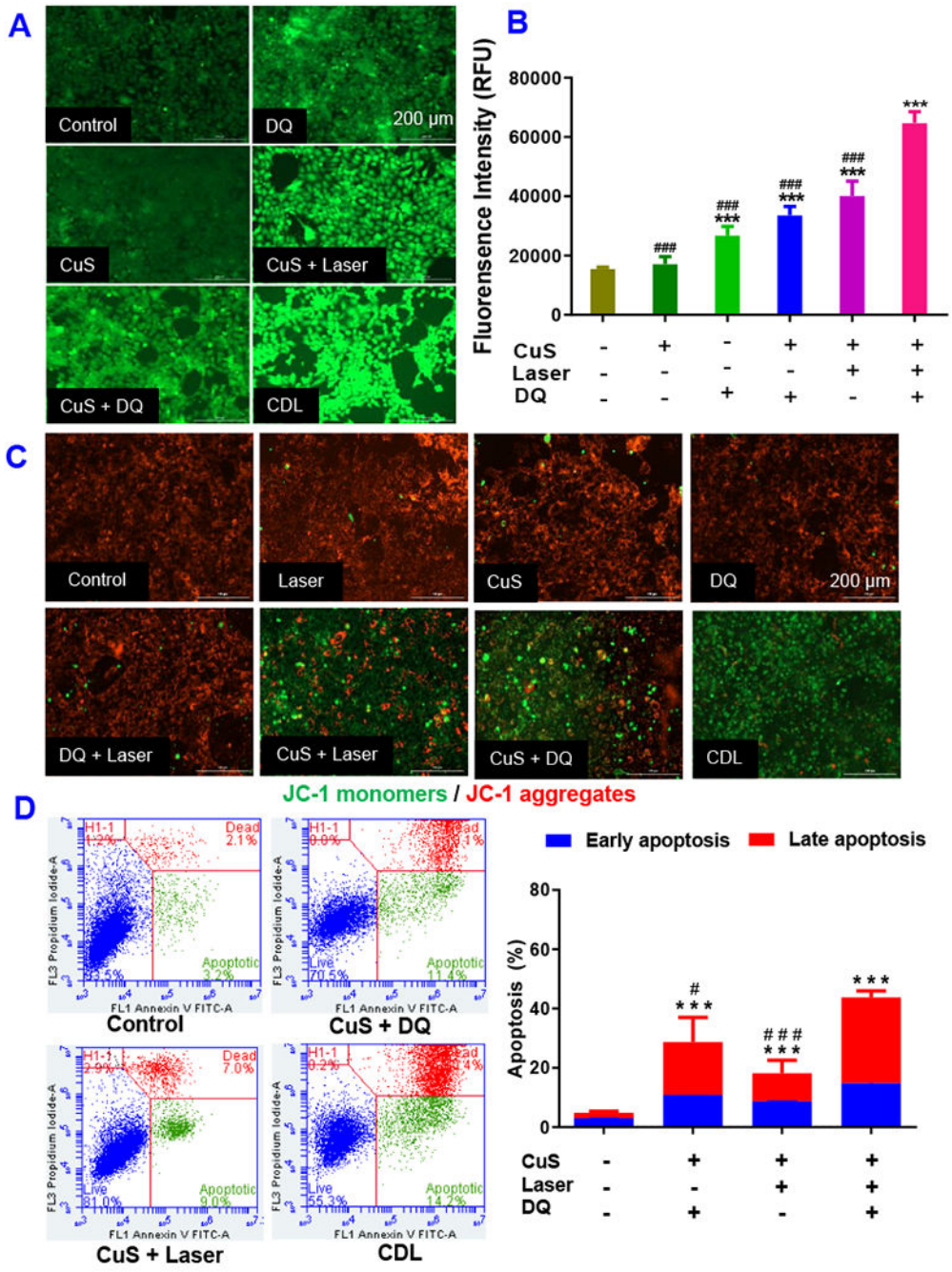

Figure 5.

Intracellular ROS levels of 4T1 cells receiving different treatments were determined with DCFH-DA dye based method. **(A)** Fluorescence image and **(B)** fluorescence intensity determined with fluorescence spectrometer. **(C)** The change of MMP was determined with JC-1 dye method. **(D)** Annexin V/PI apoptosis assay determine the percentage late-stage apoptotic cells (annexin V^+/PI^+) and early-stage apoptotic cells (annexin V^+/PI^-) with flow cytometry. (CuS, 0.1 mM; DQ, 2 μM Laser, 2.54 W/cm^2 for 5 minutes. Data are presented as

the mean ± SD, n = 3, *** $P < 0.001$ compared with the negative control. # $P < 0.05$, ### $P < 0.001$ compared with the CDL treatment group).

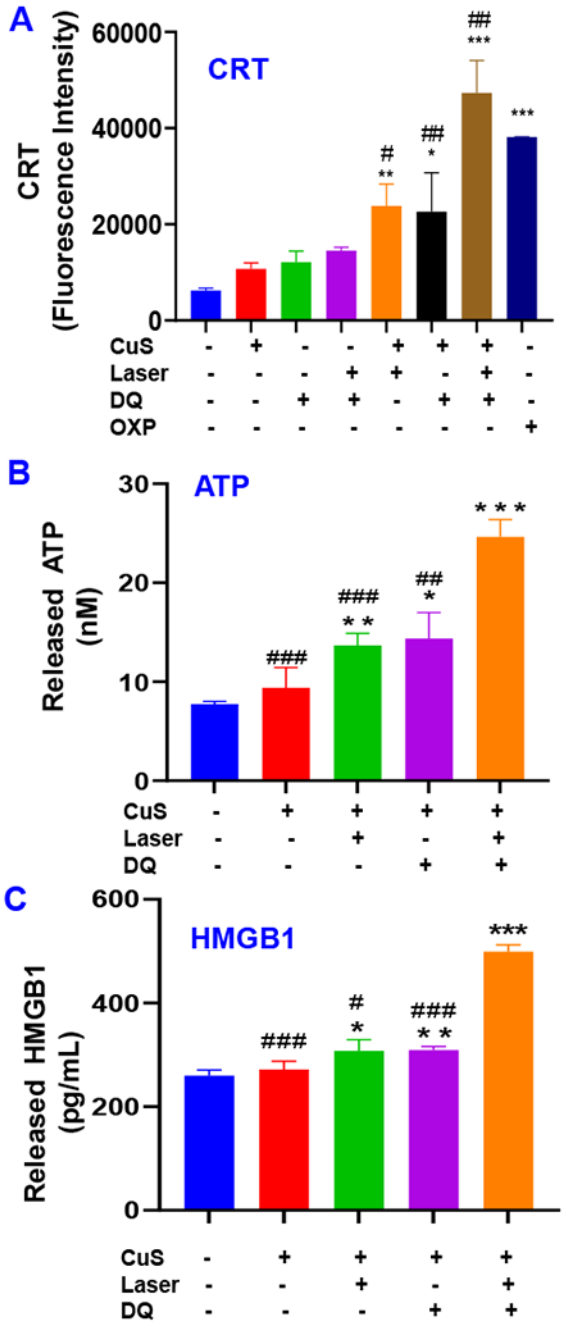

Figure 6. Biomarkers of ICD.

(A) Cell surface CRT determined with flow cytometry. **(B)** ATP release was determined with ATP bioluminescence detection kit. **(C)** HMGB1 release was determined with ELISA. (CuS, 0.1 mM; DQ, 2 μM Laser, 2.54 W/cm^2 for 5 minutes, OXP 5 μM). Data are presented as the mean ± SD, n = 3, * P < 0.05, ** P < 0.01, *** P < 0.001, compared with the negative control group; # P < 0.05, # # P < 0.01, # # # P < 0.001, compared with CDL treatment group).